Hindawi
Geofluids
Volume 2022, Article ID 9517011, 13 pages
https://doi.org/10.1155/2022/9517011

Research Article

Experimental Study of Seepage Characteristics of Filling Structures in Deep Roadway

Shaoshuai Shi,[1,2,3] **Xiangxiang Zhu**,[2] **Zhiguo Cao**,[1] **Lin Bu**,[2] **Zhijie Wen**,[4] **Zongqing Zhou**,[2] **Weidong Guo**,[2] **and Ruijie Zhao**[2]

[1]*State Key Laboratory of water Resource Protection and Utilization in Coal Mining, Beijing 100011, China*
[2]*School of Qilu Transportation, Shandong University, Jinan 250061, China*
[3]*China Railway Economic and Planning Research Institute, Beijing 100083, China*
[4]*State Key Laboratory of Mining Disaster Prevention and Control Co-Founded by Shandong Province and Ministry of Science and Technology, Shandong University of Science and Technology, Qingdao 266590, China*

Correspondence should be addressed to Xiangxiang Zhu; zhuxiangxiang@mail.sdu.edu.cn
and Zhijie Wen; wenzhijie@sdust.edu.cn

Received 6 September 2021; Revised 30 November 2021; Accepted 24 February 2022; Published 14 March 2022

Academic Editor: Richeng Liu

In order to study the seepage failure mechanism of roadway filling medium consisting of cohesive soil under complex hydrogeological conditions, a large-scale triaxial stress-seepage test system was utilized to investigate the influence of kaolin content and seepage loading rate on the seepage characteristics of filling medium. Through the analysis on the variation rules of sand loss and particle size distribution, the seepage characteristics and whole process of seepage instability of filling medium were explored in depth. It is concluded that (1) The seepage instability process of filling medium can be categorized into three stages: the initiation loss of fine clay, the accelerating loss of soil, and the stable status of soil loss. (2) The seepage failure process rate is proportional to the seepage loading rate and inversely proportional to the content of kaolin. (3) The kaolin and sand content of remaining mixture presented initial>bottom>middle>top status. The research results have guidance value for exploring the instability evolution mechanism of filling medium in deep roadway.

1. Introduction

Since the 21st century, especially with the implementation of the China Western Development and The Belt and Road Initiative, the focus of coal mining engineering or tunnel construction in China is gradually shifting to the western mountainous and karst areas with extremely complex terrain and geological conditions. Moreover, mine roof water inrush has been identified as one of the most serious dangers to mining safety and production in China [1–3]. Owing to various hydraulic and geological conditions and complex tectonic structures in deep coal mine roadway, causes and evolutionary mechanisms of mine water inrush vary significantly. [4, 5] The occurrence of mine water-mud inrush disasters in deep roadway has crypticity and burstiness, water-bearing structure(such as water-mud filling karst conduit) has the characteristics of large amount of water and sufficient water supply [6–9]. Mine water inrush disasters induced by water-bearing structures may cause casualties, economic losses, and project delay. If it is not effectively controlled, it is easy to induce environmental geological disasters such as water resources depletion and ground collapse, which seriously threatens social stability and economic development [10, 11].

At present, the key problem why mine water inrush disasters are difficult to forecast and control is that the geological conditions and catastrophic evolution process are extremely complex, which may cause that the catastrophic evolution mechanism of water inrush has not been systematically revealed. Through the case analysis of mine water inrush disasters in recent years, it is shown that the seepage instability of filling medium in fault, karst pipeline is one of

the main causes of water-mud inrush disasters in coal mine [12–14] and most of them occur in the high permeability sandy-clay filling medium. Under the action of strong seepage, the continuous erosion of the filling medium makes the seepage channel appear, gradually extends then through, and the stability of the filling medium is constantly reduced, finally resulting in the occurrence of mine water inrush disasters [15, 16].

Previous studies on mine water inrush of deep roadway have focused on the water inrush mechanism and a large amount of research has been conducted through theoretical analysis, numerical simulation, and laboratory tests [17–20]. In terms of numerical simulation, Islam and Donnelly [21, 22] established a seepage-damage coupling model to reveal that mine water inrushes are related to the action of strong seepage and stress. Yang et al. [23] developed a flow erosion model for mine water inrush to reveal variation characteristics of the pressure field, velocity field, and porosity. In theoretical analysis, Yao et al. [24] established a deformation-seepage-erosion coupling model to explore the evolutionary rules of permeability characteristics of karst collapse columns in deep roadway. Li et al. [25] put forward stress-seepage-damage coupling equation before and after damage of filling medium to reveal the catastrophe evolution mechanism of mine water inrush in filling fault. However, the aforementioned research results could hardly simulate the actual water inrush process and elucidate the physical phenomenon.

In recent years, laboratory tests play a vital role in coal mining. Scholars around the world have gained plentiful and substantial achievements in the study of seepage characteristics of cohesionless soils by means of seepage instability tests. For example, Skempton and Brogan [26] carried out the experiments to reveal the critical hydraulic gradient of fine particle migration and instability in cohesionless soils under different particle size distributions. Su et al. [27], Tomlinson and Vaid [28], and Fannin and Moffat [29] have successively adopted large-scale permeameters to carry out the internal seepage test and studied the influences of particle size distribution, permeability, and confining pressure on the seepage instability process of cohesionless soil. However, the research results mentioned above were only limited to study on seepage characteristics of cohesionless soil and there are few large-scale experimental studies on seepage instability of cohesive soil. In order to explore evolutionary rules of internal erosion instability of cohesive soil, Bendahmane carried out seepage tests to analyze the influence of hydraulic gradient and clay content on the cohesive soil erosion mechanism [30–32]. Liang and Fan [33] investigated and analyzed the important reasons for the influence of pore size on clay seepage characteristics of tiny-particle clay. Richards and Reddy [34] conducted clay seepage erosion tests in a new true-triaxial pipeline test apparatus to explore three kinds of pipeline seepage failure modes under different fine particle contents and types. Mao and Akihiro [35] carried out the permeability test of cohesive soil, using a triaxial permeability tester to explore the influence of initial fine particle content on the seepage instability process. Meng et al. [36] employed the three-dimensional model test system of mine water inrush to analyze the structural instability characteristics and seepage laws of karst conduit fillings with different permeability coefficients. However, the aforementioned research results mainly focus on the study of the seepage characteristics of cohesiveless soil. Moreover, in terms of the seepage characteristics and evolution rules of cohesive soil, no in-depth studies have been conducted.

In this study, from the perspective of mine water inrush disaster characteristics of filling structures in deep roadway, a large-scale triaxial stress-seepage test system was utilized to carry out seepage instability test on filling medium. The effects of kaolin content and loading rate on seepage characteristics and the evolution rules of grain size distribution before and after seepage are investigated, so as to reveal the variation rules of permeability characteristics and seepage instability mechanism in filling medium.

2. Preparation of Similar Materials for Seepage Failure Test

2.1. Similar Materials of Surrounding Rock

2.1.1. Primary Components of Similar Materials of Surrounding Rock. In order to simulate factual evolution process of water-mud inrush induced by seepage instability of filling medium under the in situ stress state in deep roadway, similar materials consist of fine sand, calcium carbonate, iron powder, white cement, chlorinated paraffin, and silicone oil, which satisfy strength, deformation, and permeability of native rock. Then, a large amount of similar material ratio tests were conducted to select the ideal mix proportion of similar materials. Finally, the composition ratio of various ingredients is determined and the basic parameters of surrounding rock similar materials are obtained. The specific basic parameters are shown in Table 1.

In Table 1, S: Ca: Fe: Ce: Cp: So denote, respectively, sand: calcium carbonate: iron powder: white cement: chlorinated paraffin: silicon oil. ρ represents the density, σ_c represents the compressive strength, E represents the modulus of elasticity, k represents the permeability coefficient, and K represents the softening coefficient.

2.1.2. Preparation of Surrounding Rock Specimen. In this paper, the mold for the preparation of surrounding rock specimen is designed into a detachable iron mold. Rectangular blocks can meet the requirements of the precast rectangular structure in the specimen, providing convenience for sample processing. The outer diameter and height of the large-diameter specimen prepared by the mold can reach 300 mm and 300 mm, respectively. The rectangular piping-type disaster-causing structure is simplified and prepared by rectangular precast components to penetrate. The length and width of the rectangular section are both 80 mm.

The production of surrounding rock specimen is an important link of the test, which has significant influence on the test results. Therefore, in terms of physical, mechanical, and hydraulic properties, it is required that the specimen has stable properties, certain strength, low permeability, and is convenient for large-scale preparation at room

Table 1: Mix proportion of surrounding rock similar materials and its basic parameters.

S:Ca:Fe:Ce:Cp:So	ρ/(g·cm^{-3})	σ_c/(MPa)	E/(GPa)	k/(cm·s^{-1})	K
1 : 0.08: 0.07: 0.25: 0.1 : 0.02	2.48	0.92	0.10	3.55×10^{-6}	0.69

temperature. The basic components of surrounding rock similar materials are shown in Figure 1.

The preparation process is divided into five steps.

Step 1. The aggregate and cementing agent were prepared according to the ideal mix proportion of similar materials in Table 1.

Step 2. Four fine-grained materials including sand, calcium carbonate, iron powder, and cement were mixed evenly, and then, the appropriate amount of water was added into mixture by a mixer. Subsequently, the silicone oil and chlorinated paraffin were stirred in the mixture for 8-10 minutes.

Step 3. The stirred similar materials were added to the mold above and the single-layer cylindrical compaction was used to achieve a surrounding rock specimen.

Step 4. The specimen needed to be maintained at room temperature for 7 days, till then, the preparation of a large-diameter surrounding rock specimen containing disaster-causing structure was completed.

2.2. Similar Materials of Filling Medium

2.2.1. Primary Components of Filling Medium Similar Materials. With the water-bearing structures and unfavourable geological bodies exposed, the water-blocking structure consisting of cohesive soil, fine sand, and gravel is considered as the filling medium [25, 37]. Filling medium structure of deep roadways is the last barrier water-mud inrush disaster, the composition characteristics and mechanical properties are the key factors to affect its stability. However, the gushed filling medium is significantly different from initial fillings in physical and mechanical properties. Moreover, there are difficulties in sampling and maintaining for gushed filling medium, which is hard to apply to a large number of laboratory tests.

The penetration of filling medium induced by the continuous loss of clay and sand under seepage leads to the instability of filling medium structure and water-mud inrush disaster. Through the analysis of the samples of mud and sand gushed from the water-mud inrush cases, the gushed filling medium are mainly composed of gravel, fine sand, and clay. Therefore, the fine sand and clay with different grain compositions, used as filling particles of different grain sizes, are mixed uniformly to serve as filling material in the disaster-causing structure. Furthermore, the particles of which grain size is finer than 0.075 mm were replaced by kaolin.

2.2.2. Essential Properties of Filling Medium Similar Materials. The permeability and mechanical properties of filling medium play a key role and have a significant effect on the formation of internal seepage channel and instability evolution process. Therefore, in order to simulate the filling medium with different mechanical and permeability characteristics, three different mix proportions of filling medium similar materials were used to carry out seepage tests by adjusting the content of kaolin and sand. As is shown in Figure 2, the filling medium similar materials were prepared in this paper according to material composition and grain size distribution. The specific grain size distribution is shown in Table 2.

3. Test on Seepage Failures of Filling Medium

3.1. A Large-Scale Test System for Coupled Seepage and Triaxial Stress. As is shown in Figure 3, a self-developed large-scale triaxial stress-seepage test system was adopted to conduct permeability characteristics test on filling medium in rectangular disaster-causing structure. This test system consists of a visualization triaxial press chamber, particle loss collecting system, and a real-time data acquisition and monitoring system. Then, a visualization triaxial press chamber, which can truly simulate triaxial compression and hydraulic state of filling medium, includes confining pressure, axial pressure, and seepage pressure loading system. The pressure chamber, equipped with a real-time camera, adopts transparent acrylic material to realize high visual degree, which can meet the requirement of real-time monitoring of sample changes during test.

3.2. Test Scheme and Procedures

3.2.1. Design of Test Scheme. In order to explore the evolution rules of internal strength, permeability, and mechanical properties of fillings in the process of seepage instability, the tests focus on the influence of two parameters (kaolin content in the filling medium and seepage pressure loading rate) on the seepage instability of filling medium. As shown in Table 3, the tests are divided into six working conditions.

According to Table 2, the sand and kaolin are mixed together to prepare the corresponding gradation filling medium. As Tests 1, 3, and 5, the seepage pressure loading rate is fixed and the content of kaolin is adjusted. In rectangular cross-section karst pipeline of internal size 80 mm × 80 mm × 300 mm, the influence of kaolin content on the permeability of filling medium is analyzed under the condition of 100 kPa axial compression and 200 kPa confining pressure.

Meanwhile, the seepage rate has a great influence on the seepage failure of the filling medium, so it is vital to investigate the influence of seepage pressure loading rate on the seepage process in the experimental process. As Tests 1 and 2, filling medium with the same particle size distribution

Figure 1: Basic components of similar material of surrounding rock.

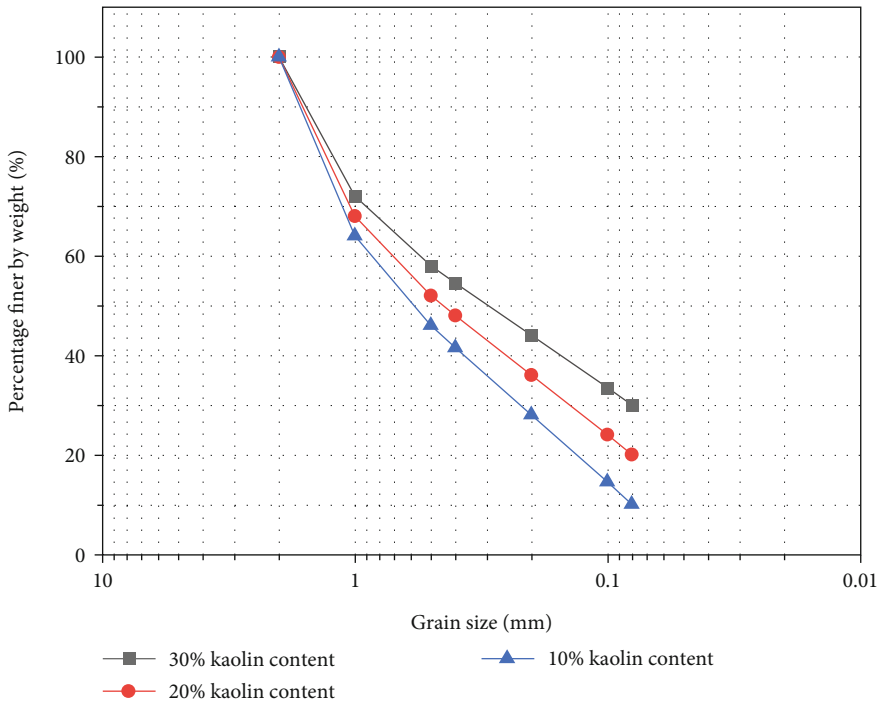

Figure 2: Grading curves of filling medium with different kaolin contents.

Table 2: Basic components of clay-sand-type filling medium.

Kaolin	Grain size composition Sand					
<0.08 mm	0.08-0.1 mm	0.1-0.2 mm	0.2-0.4 mm	0.4-0.5 mm	0.5-1 mm	1-2 mm
30.0%	3.5%	10.5%	10.5%	3.5%	14.0%	28.0%
20.0%	4.0%	12.0%	12.0%	4.0%	16.0%	32.0%
10.0%	4.5%	13.5%	13.5%	4.5%	18.0%	36.0%

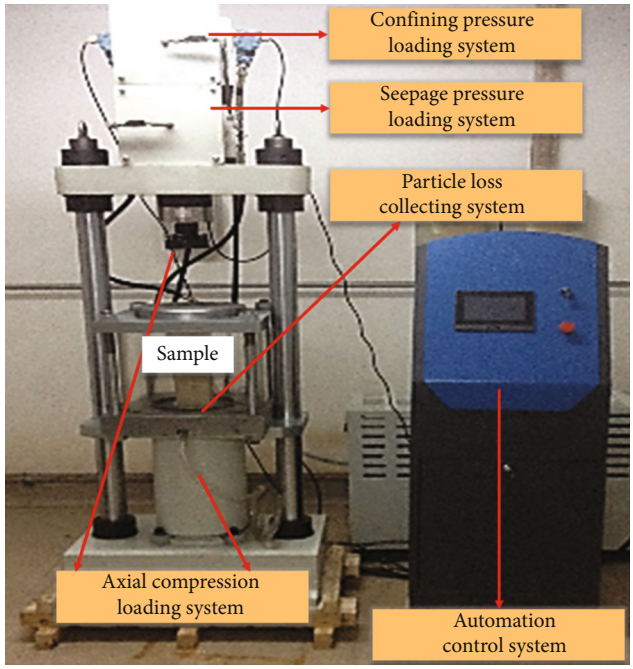

Figure 3: A large-scale triaxial stress-seepage test system.

Table 3: Test conditions.

Test number	Kaolin content %	Loading rate MPa/min
1	30	0.01
2	30	0.08
3	20	0.01
4	20	0.08
5	10	0.01
6	10	0.08

was prepared, by changing seepage pressure loading rates, the permeation characteristics of filling medium were going to be analyzed under the condition of 100 kPa axial compression and 200 kPa confining pressure. The loading schemes of permeability tests are shown in Table 4.

Having the seepage test completed, the remaining filling medium in the rectangular mold is analyzed. The top, middle, and bottom parts of the fillings are sampled, respectively, to analyze the changes of particle size distribution before and after the seepage failure of the filling medium.

3.2.2. Model Test Procedures. The permeability test process is summarized below.

Step 1. Preparation of test system. Firstly, the preparation of the triaxial stress-seepage test system is installed; then, a 2 mm filter is laid on a funnel-shaped particle loss collecting device. The sealing ring is placed around the large diameter of the rectangular base and the funnel to isolate the water and air in the confining pressure system and the specimens prepared by similar materials of surrounding rock are placed on the top.

Step 2. Construction of the filling material. The filling material is prepared on the basis of grain size composition in Table 2, and then, the filling material with uniform mixing is packed into the precasted structure in the light of 20-30 mm per layer. Each layer of filling medium is separately paved and compacted. When the filling medium height reaches 150 mm, Φ0.6 mm glass beads are laid at the top of the filling medium to form a uniform flow of injected water.

Step 3. Seal the test system. Subsequently, installing cover and round seal ring under it is to seal visual pressure chamber. In order to seal the whole device, the upper and lower cover plates are pressed by setting up four pull rod bolts. The automation control system is operated to load axial compression to design value, which completes the sealing of upper and lower cover plate and specimen.

Step 4. Saturate the specimen and sample. In order to make the specimen saturated, the water pressure loading system is adjusted to 10 kPa for some time to discharge air in the sample. When the sample is saturated, computer system is operated for loading confining pressure to the design value at a certain rate. The schematic diagram of a test system is shown in Figure 4.

Step 5. Loading of seepage pressure. So far, the preparation work in the early stage of the test is completed. Then, the permeability test of fillings for rectangular disaster-causing structure is conducted. The computer system is operated to start seepage pressure loading on the basis of loading scheme in Table 4. To ensure the seepage instability failure of the filling medium, the final pressure is set to 2 MPa.

Step 6. Collection and sampling of mixture. Water bottles are used to collect the sandy-clay mixture at the bottom of the device and replaced every minute to ensure that the mixture is collected at the same time interval. After completing the seepage test, the top, middle, and bottom parts of the filling medium are sampled, respectively.

4. Result Analysis of the Test

When the rectangle structure is filled with 10%, 20%, and 30% kaolin, the collected mixture condition is shown in Figure 5.

4.1. Effect of Kaolin Content on Permeability Characteristics

4.1.1. Sand and Clay Loss Analysis. In the process of permeability instability test on filling medium, water flowing from the bottom of the sample is collected every 60s, and the sandy-clay mixtures of the six groups of tests are loaded into transparent plastic bottles at the same time interval. Furthermore, in order to carry out wet and dry separation, the sand and clay effluent in each bottle is poured into disposable paper cup and then put into an oven adjusted to 50°C for

Table 4: Loading schemes of permeability tests.

Type of loading	Loading pressure (kPa/min)	Pressure type	Loading mode
Axial compression	14	Hydraulic fluid	Continuous loading to the design value
Confining pressure	30	Water hydraulic	Continuous loading to the design value
Seepage pressure	10/80	Water hydraulic	Gradually applied load to the failure of filling medium

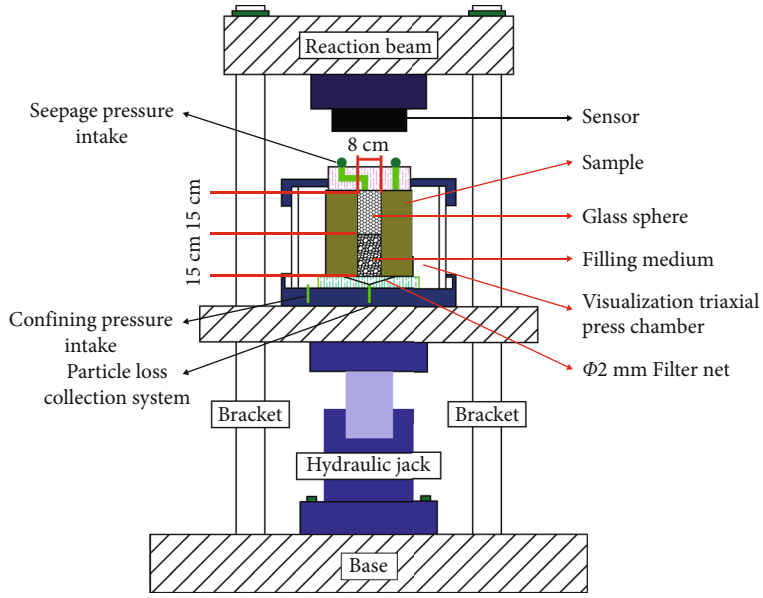

Figure 4: Schematic diagram of a test system.

24 h, to ensure that the water in the mixture has been completely removed and the mass of it in each stage is weighed. The specific amount of sandy-clay mixture is shown in Table 5.

Figure 6 shows the variation curves of cumulative sand inflow versus time for three kinds of kaolin content in the sandy-clay type filling medium. With the development of the seepage failure process of filling medium, the cumulative sand loss with the increasing of time shows "S" growth curve, and ultimately, the sand loss rate is reduced to zero. In terms of 20% or 30% kaolin content samples, in the first stage, some fine particles begin to flow out. Meanwhile, the sand inflow and growth rate are very low and the water quality is clear (see bottles 1 and 2 in Figures 5(a) and 5(b)). In the second stage, the cumulative sand-clay mixture loss shows a steep increase trend in 2 ~ 3 minutes. The water quality has changed from clear to turbid, as shown in bottles 3 and 4 in Figures 5(a) and 5(b). With a sandy-clay mixture inflow increasing sharply, the growth rate also becomes very large. The fine particles gush out of the filling medium with the flow, so as to decrease its permeability. Further, the larger particles inside filling medium began to slip, and the fine particles have been exhausted. In the third stage, the water quality gradually recovers from turbidity to clarity 4 minutes, as shown in bottles 5 to 8 in Figures 5(a) and 5(b). Compared with the high sand and clay loss rate in the initial stage, with the most fine sand and clay flowing out in the filling medium, only large skeleton sand is left. Eventually, the sand and clay loss rate decreases close to zero. The cumulative sand inflow curve of the water inrush process is close to the level, and the total amount of sand and clay loss tends to be stable. However, under the condition of kaolin content of 10%, the variation trend of cumulative sand inflow also presents the same trend, but the variation trend is not that obvious. As a result of low content of fine particles and large distance between soil particles, the interaction force is small, which slightly hinder the permeability process. Therefore, the filling medium in the structure is easy to be carried by the water to form a complete seepage channel, which leads to seepage instability and failure in advance.

Through comparative analysis, it can be concluded that the accumulative loss amounts of sandy-clay mixture in filling medium increase with the increase of time, and finally, the growth rate decreases close to zero. With the increase of kaolin content, the cumulative and ultimate amount of clay-sand increased in the same time period. With the decrease of kaolin content, the time point of sharp increase of sand and clay loss is advanced, which accelerates the process of seepage failure and destruction of filling medium.

4.2. Effect of Seepage Pressure Loading Rate on Permeability Characteristics

4.2.1. Sand and Clay Loss Analysis. Figure 7 shows the variation curve of cumulative sand-clay loss with time under two

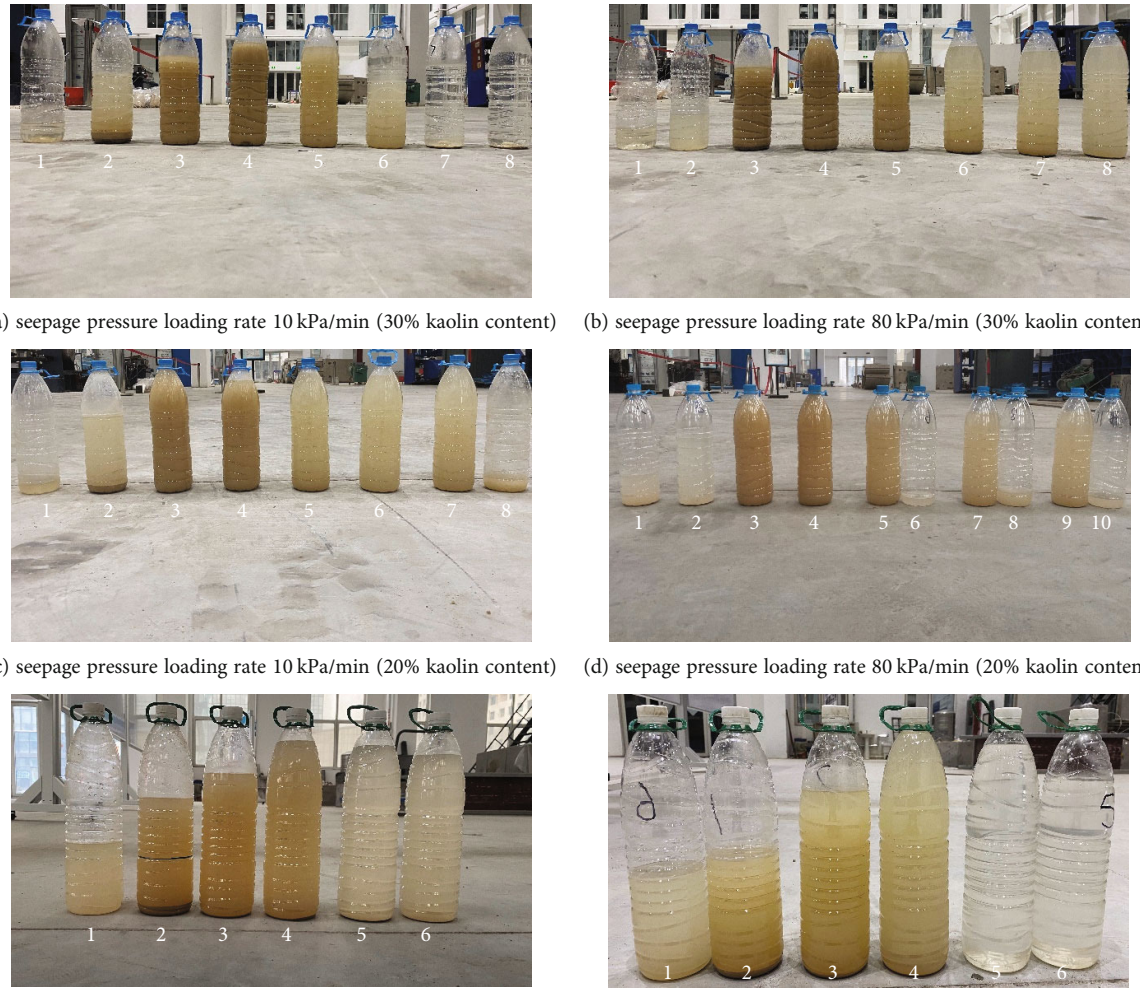

(a) seepage pressure loading rate 10 kPa/min (30% kaolin content)
(b) seepage pressure loading rate 80 kPa/min (30% kaolin content)
(c) seepage pressure loading rate 10 kPa/min (20% kaolin content)
(d) seepage pressure loading rate 80 kPa/min (20% kaolin content)
(e) seepage pressure loading rate 10 kPa/min (10% kaolin content)
(f) seepage pressure loading rate 80 kPa/min (10% kaolin content)

Figure 5: Water quality condition during the process of water inrush from filling medium.

Table 5: Statistics of sand production in each bottle.

Test number	Seepage pressure loading rate MPa/min	Kaolin content %	Loss amounts of sandy-clay mixture g								Total amounts of sandy-clay mixture g
			1 min	2 min	3 min	4 min	5 min	6 min	7 min	8 min	
1	0.01	30	6.5	17.8	43.0	14.9	8.6	5.2	4.2	3.9	104.1
2	0.08	30	8.4	25.6	61.0	15.7	6.5	6.6	4.8	2.4	131.0
3	0.01	20	3.4	15.7	41.4	6.8	5.1	3.0	2.0	/	77.4
4	0.08	20	2.5	14.0	54.9	9.6	8.3	7.9	3.2	/	100.4
5	0.01	10	0.1	16.0	10.0	2.0	1.0	0.1	/	/	29.2
6	0.08	10	0.1	24.2	25.0	11.0	7.0	2.0	/	/	69.3

seepage pressure loading rates. The loading seepage pressure is comparatively small at 1 min, so the sand and clay loss remains at a very low level and only a few fine sand and clay gush out in the course of the test. It can be inferred that the finer particles are easier to reach the initial migration speed at the same seepage pressure loading rate. When the time is 2 min, as seepage pressure increases, the amount of gushing sand and clay begins to increase gradually. As fine particles continue to lose, the permeability increases, and the internal seepage channel begins to expand gradually; then, the relatively large particles begin to leave the filling medium, which represents the end of the first stage of the whole process. The second stage shows in 2-4 min that the sand and clay losses begin to accelerate significantly due to the expansion of seepage failure process. Meanwhile, the difference of cumulative sandy-clay mixture

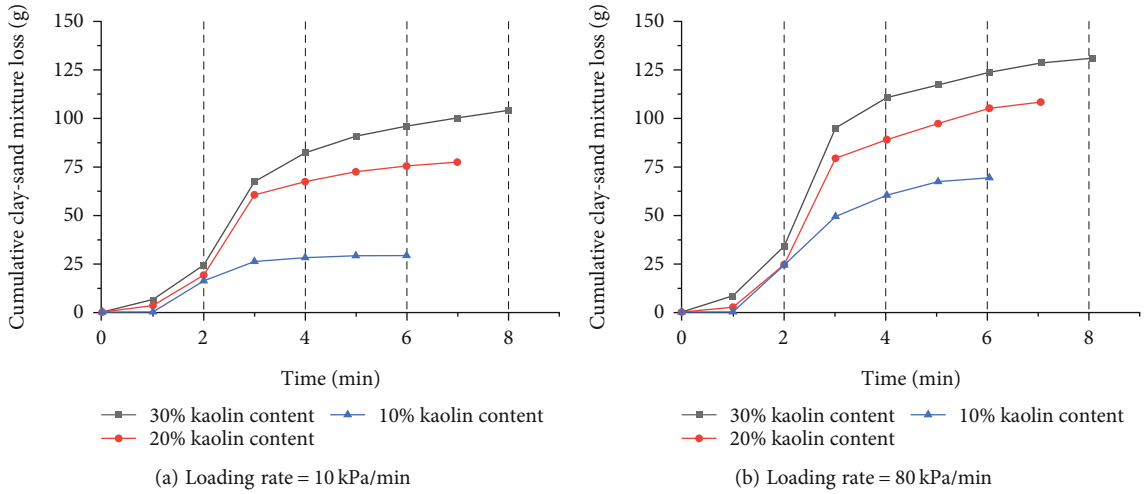

Figure 6: Variation curves of cumulative sandy-clay mixture loss for different kaolin contents.

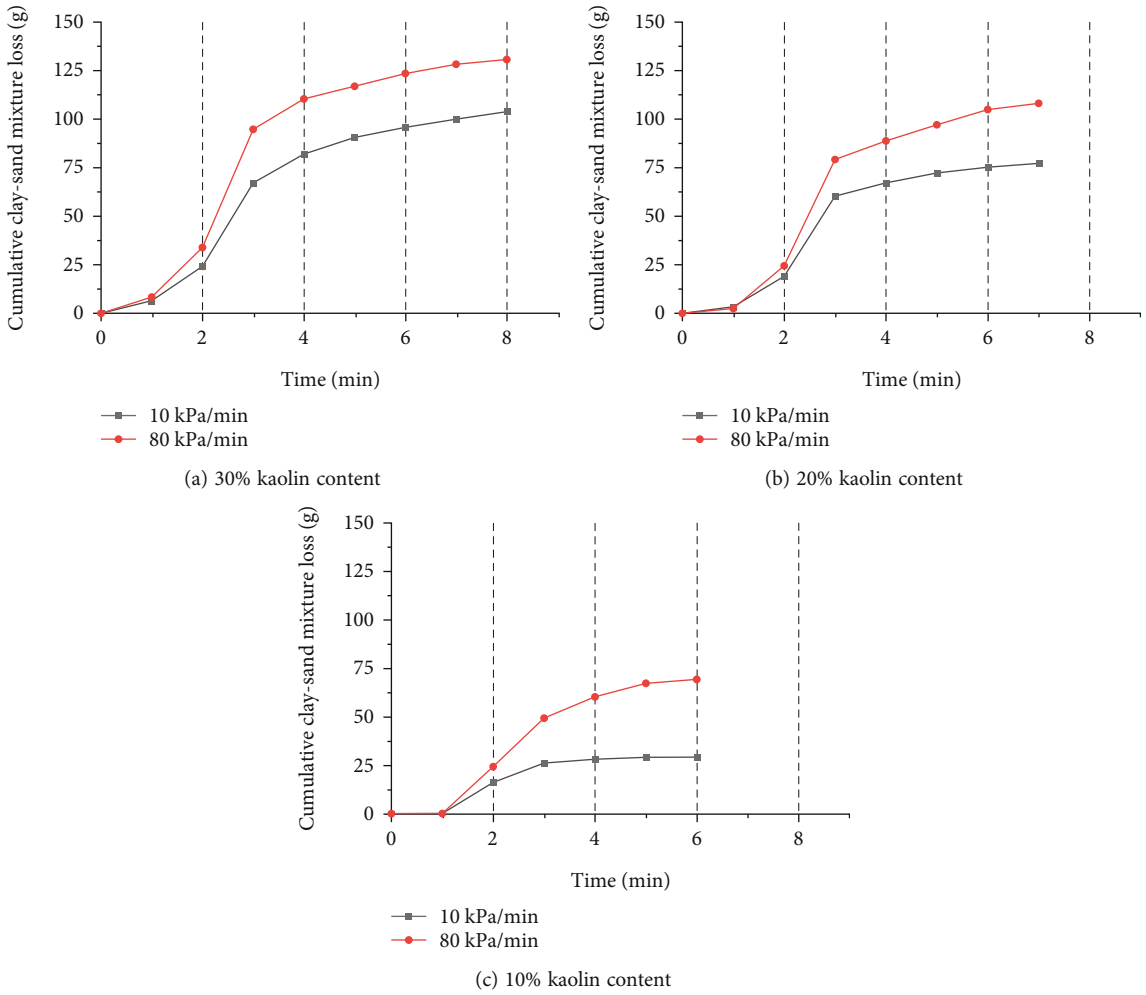

Figure 7: Variation curves of cumulative clay-sand mixture loss for different seepage pressure loading rates.

loss under different loading rates is expanding, which indicates that the seepage channel is gradually formed in filling medium. However, with the continuous loss of fine particles, the loss rate decreases sharply. Then, the third stage begins at 4 min, the sand and clay loss rate slowly decreases and the curve tends to be horizontal, which means the

whole mixture of filling medium is lost except for large skeleton sand, a complete seepage channel network has formed.

Based on the analysis, the following conclusions can be drawn: firstly, with the increase of the seepage loading rate, the cumulative amount of mixture loss in the same period and the final state are greater; secondly, with the increase of seepage loading rate, the time point of sharp increase of mixture loss is advanced, which accelerates the process of seepage damage of filling medium.

4.3. Analysis on Particle Size Distribution of Filling Medium. Due to the migration of particles in the filling medium, the materials composed of still existing soil particles in the rectangular piping-type structure are called remaining mixture. At the end of the experiment, samples from remaining mixture of six tests are taken from the top, middle, and bottom of the structure. They are, respectively, put into disposable paper cups and then placed in the oven adjusted to 50°C for 24 hours to make sure the water is completely removed. Subsequently, the screening test is carried out on the dried sample. The pore sizes of sieve set are 0.08 mm, 0.1 mm, 0.2 mm, 0.4 mm, 0.5 mm, 1 mm, and 2 mm, respectively. After setting the sleeve into a shaker for 10 min, the weight of each sieve is to be weighed. The particle grading variation curves of remaining filling medium are shown in Figures 8–13. In this paper, the particle sizes (0 ~ 0.4 mm) are defined as fine particles and the particle sizes (0.4 ~ 2 mm) are defined as coarse particles. The content of particles represents weight percentage in a certain particle size range.

4.3.1. Analysis on Particle Size Distribution of Remaining Mixture with a 30% Kaolin Content. According to Figures 8 and 9, the particle gradation curves of the remaining mixture compared with those of initial status, the fine particle contents all decrease and the content of particles larger than 0.4 mm all increases.

When the seepage pressure loading rate is 10 kPa/min, the contents of particle sizes smaller than 0.08 mm, 0.08-0.1 mm, and 0.1-0.2 mm decrease, and the other particle size contents increase at the top, middle, and bottom parts of remaining mixture. As shown in Figure 8, the amount of particle size smaller than 0.08 mm in the top and middle of the filling medium decreases significantly. On the contrary, the contents of coarse particles apparently increase. The content of fine particles in the filling medium decreases slightly, which has little effect on the particle size composition of each part. When loading the seepage pressure at 80 kPa/min, similar to the loading rate of 10 kPa/min, the contents of particle size smaller than 0.2 mm also decrease and the other particle size contents increase as well. However, the difference is that the particle size of 0.4 mm-0.5 mm, 0.5 mm-1 mm, and 1-2 mm increase more dramatically than that of 10 kPa/min.

On the whole, the permeation process of filling medium with high clay content is most significantly affected by fine particles. In the initial stage of water seepage in filling medium, the clay and fine sands start to move in the pores shaped by coarse sand, leading to the reduction of the cohesion between particles. As more and more fine particle loss, the permeability and the pore water pressure increase, resulting in the expansion of the internal seepage channel of the filling medium. Migrated particles at the middle and bottom parts of the sample are fewer and relatively stable than the top part. The clay and fine sands in the top part are easier to lose under the action of seepage; hence, the loss amounts of migrated fine particle are the largest, which is contrary to coarse particles. Along with the gradual expansion of the seepage channel and water flow rate increases, the stability of the whole specimen is greatly weakened, making it more difficult to resist the seepage. Under the action of their own gravity and seepage, the fine particles at the top and middle parts of filling medium start moving to bottom part of kaolin-sand mixture and replace lost fine particles to form 'supplying-particles' at the bottom of filling medium. Except for a large number of fine particles, only a small number of coarse particles begin to gush out from the mixture and the seepage channel has formed. Therefore, the loss of fine particles in the top remaining mixture is the most, the coarse particles is the least, and the loss of fine particles in the lower part is the least.

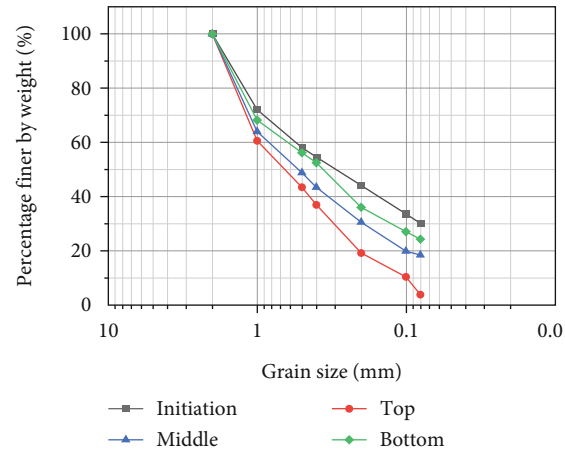

Figure 8: Test number 1 particle grading variation curves before and after seepage.

Through comparative analysis above, it can be summarized as follows: (1) Compared with the initial status of filling medium, the fine particle content of the remaining mixture decreases and the content of coarse particles increases. (2) With other conditions unchanged, when the seepage loading rate is greater, the content of coarse particles in each part is higher; conversely, the fine particle content is lower. (3) With the increase of loading rate, the seepage failure process of filling medium is aggravated. It can be inferred that the loss of fine particles leads to the decrease of internal cohesion and the loss of coarse particles is relatively increased. (4) With other conditions unchanged, contrary to 0.4-2 mm coarse particles, the change of fine particles content of remaining mixture presents initial>bottom>middle>top status.

4.3.2. Analysis on Particle Size Distribution of Remaining Mixture with a 20% Kaolin Content. According to

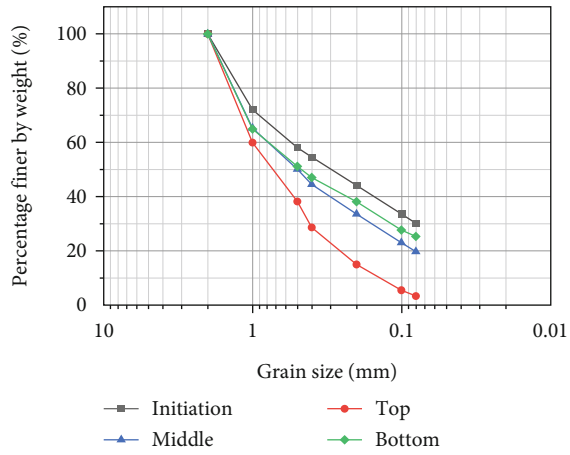

Figure 9: Test number 2 particle grading variation curves before and after seepage.

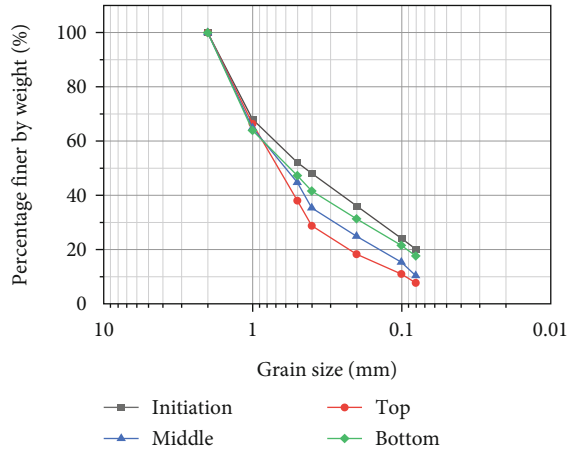

Figure 10: Test number 3 particle grading variation curves before and after seepage.

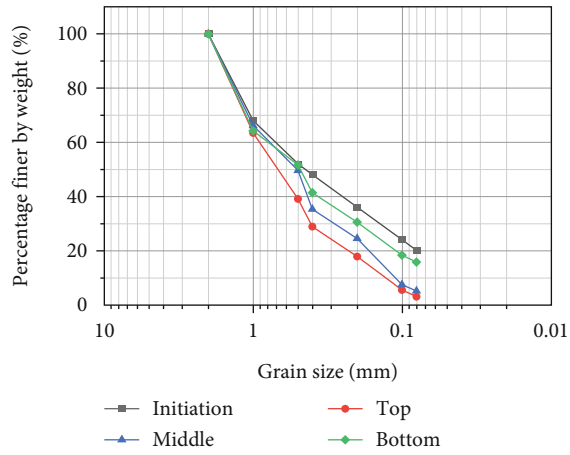

Figure 11: Test number 4 particle grading variation curves before and after seepage.

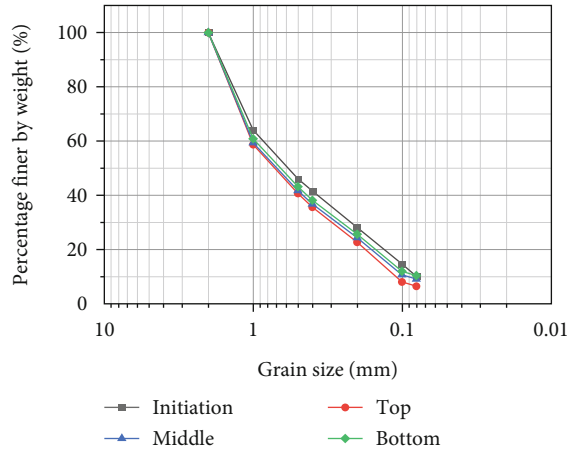

Figure 12: Test number 5 particle grading variation curves before and after seepage.

Figures 10 and 11, the particle gradation curves of the remaining mixture in tests 3 and 4, compared with those of initial status, the fine particles contents all decrease and the content of coarse particles all increases.

When the seepage pressure loading rate is 10 kPa/min, the contents of particle sizes smaller than 0.08 mm, 0.08-0.1 mm, 0.1-0.2 mm, and 0.2-0.4 mm all decrease and the other particle size contents increase at the top, middle, and bottom part of remaining mixture. As can be seen from Figure 10, the content of particle sizes smaller than 0.08 mm decreases dramatically and particle sizes of 0.4 mm-0.5 mm and 0.5 mm-1 mm are opposite at the top and middle of remaining mixture. When the seepage pressure is 80 kPa/min, similar to the loading rate of 10 kPa/min, the contents of particle size smaller than 0.2 mm also decrease and contents of coarse particles increase as well. The distinction is that the particle size smaller than 0.1 mm lower and 0.4 mm-0.5 mm, 0.5 mm-1 mm increases more dramatically than that of 10 kPa/min.

As can be seen from Figures 10 and 11, there is a cross-over phenomenon in the particle gradation curves regarding to the top and middle remaining mixture, indicating that low seepage loading rate and the bonding effect between particles prevent initially internal fine particles from moving. With the increase of seepage loading rate, the seepage water fails to flow out from the seepage channels in time, which leads to local collapse of filling medium and block the original seepage channel. Hence, the seepage water with fine particles gushes out of the new seepage channel, resulting in the decrease of the content of fine particles, and consequently, the phenomenon above occurs.

Moreover, under the circumstance of local collapse of filling medium, particles of a certain size have been flushed with seepage water no matter how large they are. Consequently, gap-graded remaining mixtures have appeared in lack of particles of a certain size.

4.3.3. Analysis on Particle Size Distribution of Remaining Mixture with a 10% Kaolin Content. According to Figures 12 and 13, the particle gradation curves of the remaining mixture in Tests 5 and 6, compared with those

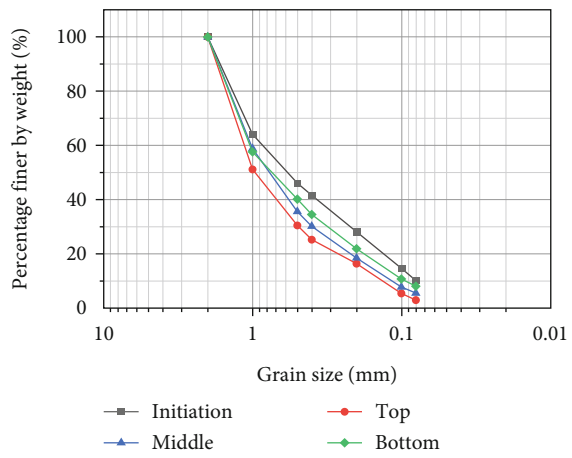

FIGURE 13: Test number 6 particle grading variation curves before and after seepage.

of initial status, the fine particle contents all decrease and the loss is more uniform. Similarly, the contents of particles larger than 0.5 mm all increase.

When the seepage pressure loading rate is 10 kPa/min, the contents of particle sizes smaller than 0.08 mm, 0.08-0.1 mm decrease and the contents of particle sizes 0.1-0.2 mm, 0.2-0.4 mm, and 0.4-0.5 mm show no significant change at the top, middle, and bottom part of remaining mixture. Furthermore, the contents of other particle size increase. Combined with Table 2, it can be inferred that the contents of particle sizes smaller than 0.1 mm reduce evenly and 1-2 mm rises dramatically. While loading rate is 80 kPa/min, the contents of fine particles all decrease, 0.4-0.5 mm has no significant change and the contents of other particle size increase.

Given the above, the fine particles of filling medium with low clay content have no significant influence on the seepage instability process. Due to the low kaolin content, the cohesion of filling medium with many large pores is comparatively small. Only a few fine particles gush out from the mixture, seepage channel has formed and seepage instability process is completed. Hence, compared with those of initial status, the tendency of particle size distribution curves of the top, middle, and bottom part of remaining mixture is basically consistent. Furthermore, the contents of particle size in each part have no significant changes.

Through comparative analysis above, it can be summarized as follows: (1) As the content of kaolin decreases, the content of fine particles in the remaining mixture also decreases and the distribution is more uniform. (2) The content of coarse particles drops more significantly as the content of kaolin decreases. (3) With the decrease of kaolin content, the effect of loading rate on particle size distribution is weakened. (4) With other conditions unchanged, contrary to coarse particles, the change of fine particles content of remaining mixture presents initial> bottom>middle>top.

5. Conclusions

A large-scale triaxial stress-seepage test system was utilized to conduct the seepage instability tests of filling-type disaster-causing structures. The changes of sand and clay loss and particle size distribution in the process of seepage instability were investigated in depth. The variation rules of seepage characteristics and the evolutionary process of seepage instability were revealed. Based on the aforementioned analysis, the results obtained in this paper can be summarized as follows.

(1) According to the evolution rules of clay-sand mixture loss, the seepage instability process of filling medium can be categorized into three stages: the initial seepage stage with very small number of fine particles loss, the accelerating seepage stage with large number of fine particles loss, and the stable stage with the whole sample collapse

(2) The effects of kaolin content and seepage pressure loading rate on the permeability of filling medium were investigated in depth. The seepage failure process rate is proportional to the seepage loading rate and inversely proportional to the content of kaolin

(3) The mutual promotion between stress-seepage erosion and particle loss is the internal cause of seepage instability. And the seepage instability process of filling medium with different kaolin contents is most significantly affected by fine particles. The change of fine particle contents of remaining mixture is consistent, presenting initial>bottom>middle>top status. Under higher seepage pressure loading rate, the lower kaolin content in the filling medium is , the more obvious phenomenon of fine particles loss in the remaining mixture is.

Data Availability

The data used to support the findings of this study are available from the corresponding author upon request.

Conflicts of Interest

The authors declare that they have no conflicts of interest.

Acknowledgments

This work was supported by the Open Fund of State Key Laboratory of Water Resource Protection andUtilization in Coal Mining(GJNY-18-73.3), Taishan Scholar Foundation of Shandong Province (Grant No.tsqn202103002), and the Key Research and Development Project of Shandong Province(Grant no.2019GSF111018).

References

[1] B. Hebblewhite, "Fracturing, caving propagation and influence of mining on groundwater above longwall panels-a review of

predictive models," *International Journal of Mining Science and Technology*, vol. 30, no. 1, pp. 49–54, 2020.

[2] H. B. Bai, D. Ma, and Z. Q. Chen, "Mechanical behavior of groundwater seepage in karst collapse pillars," *Engineering Geology*, vol. 164, pp. 101–106, 2013.

[3] B. Y. Zhang, H. B. Bai, and K. Zhang, "Seepage characteristics of collapse column fillings," *International Journal of Mining Science and Technology*, vol. 26, no. 2, pp. 333–338, 2016.

[4] W. J. Sun, Q. Wu, H. L. Liu, and J. Jiao, "Prediction and assessment of the disturbances of the coal mining in Kailuan to karst groundwater system," *Physics and Chemistry of the Earth*, vol. 89-90, pp. 136–144, 2015.

[5] Y. M. Qi, M. Z. Li, K. J. Li, and T. C. J. Yeh, "Spatiotemporal development of mine water inrush and its mechanism—a case study in Ganhe coal mine, Shanxi, China," *Arabian Journal of Geosciences*, vol. 10, no. 19, 2017.

[6] Q. H. Qian, "Challenges faced by underground projects construction safety and countermeasures," *Chinese Journal of Rock Mechanics and Engineering*, vol. 31, no. 10, pp. 1945–1956, 2012.

[7] S. C. Li, Y. H. Qi, Z. F. Li, H. Y. Li, and J. Zhang, "A novel treatment method and construction technology of the pipeline gushing water geohazards in karst region," *Tunnelling and Underground Space Technology*, vol. 113, p. 103939, 2021.

[8] H. B. Fan, Y. H. Zhang, S. Y. He, K. Wang, X. L. Wang, and H. Wang, "Hazards and treatment of karst tunneling in Qinling-Daba mountainous area: overview and lessons learnt from Yichang–Wanzhou railway system," *Environmental Earth Sciences*, vol. 77, no. 19, 2018.

[9] S. Alija, F. J. Torrijo, and M. Ouinta-Ferreira, "Geological engineering problems associated with tunnel construction in karst rock masses: the case of Gavarres tunnel (Spain)," *Engineering Geology*, vol. 157, pp. 103–111, 2013.

[10] S. C. Li, Z. H. Xu, X. Huang et al., "Classification, geological identification, hazard mode and typical case studies of hazard-causing structures for water and mud inrush in tunnels," *Chinese Journal of Rock Mechanics and Engineering*, vol. 37, no. 5, pp. 1041–1069, 2018.

[11] S. C. Li, S. S. Shi, L. P. Li, J. Chen, Z. H. Xu, and Z. Q. Zhou, "Control of water inrush in typical karst tunnels in three gorges reservoir area and its application," *Chinese Journal of Rock Mechanics and Engineering*, vol. 33, no. 9, pp. 1887–1896, 2014.

[12] S. S. Shi, L. Bu, S. Li et al., "Application of comprehensive prediction method of water inrush hazards induced by unfavourable geological body in high risk karst tunnel: a case study," *Geomatics, Natural Hazards and Risk*, vol. 8, no. 2, pp. 1407–1423, 2017.

[13] Y. G. Xue, F. M. Kong, S. C. Li et al., "Water and mud inrush hazard in underground engineering: Genesis, evolution and prevention," *Tunnelling and Underground Space Technology*, vol. 114, p. 103987, 2021.

[14] S. C. Li, K. Wang, L. P. Li, Z. Q. Zhou, S. S. Shi, and S. Liu, "Mechanical mechanism and development trend of water-inrush disasters in karst tunnels," *Chinese Journal of Theoretical and Applied Mechanics*, vol. 49, no. 1, pp. 22–30, 2017.

[15] Z. Q. Zhou, L. P. Li, S. S. Shi et al., "Study on tunnel water inrush mechanism and simulation of seepage failure process," *Rock and Soil Mechanics*, vol. 41, no. 11, pp. 3621–3631, 2020.

[16] L. P. Li, W. F. Tu, S. S. Shi, J. X. Chen, and Y. H. Zhang, "Mechanism of water inrush in tunnel construction in karst area," *Geomatics, Natural Hazards and Risk*, vol. 7, Supplement 1, pp. 35–46, 2016.

[17] P. Bukowski, "Water hazard assessment in active shafts in upper Silesian Coal Basin mines," *Mine Water and the Environment*, vol. 30, no. 4, pp. 302–311, 2011.

[18] N. Rapantova, S. Krzeszowski, A. Grmela, and C. Wolkersdorfer, "Quantitative assessment of mine water sources based on the general mixing equation and multivariate statistics," *Mine Water and the Environment*, vol. 31, no. 4, pp. 252–265, 2012.

[19] L. Surinaidu, V. Rao, and G. Ramesh, "Assessment of groundwater inflows into Kuteshwar limestone mines through flow modeling study, Madhya Pradesh, India," *Arabian Journal of Geosciences*, vol. 6, no. 4, pp. 1153–1161, 2013.

[20] K. Polak, K. Rozkowski, and P. Czaja, "Causes and effects of uncontrolled water inrush into a decommissioned mine shaft," *Mine Water and the Environment*, vol. 35, no. 2, pp. 128–135, 2016.

[21] L. J. Donnelly, "A review of coal mining induced fault reactivation in Great Britain," *Quarterly Journal of Engineering Geology and Hydrogeology*, vol. 39, no. 1, pp. 5–50, 2006.

[22] M. R. Islam, D. Hayashi, and A. B. M. Kamruzzaman, "Finite element modeling of stress distributions and problems for multi-slice longwall mining in Bangladesh, with special reference to the Barapukuria coal mine," *International Journal of Coal Geology*, vol. 78, no. 2, pp. 91–109, 2009.

[23] B. Yang, T. H. Yang, and J. Hu, "Numerical simulation of non-darcy flow caused by cross-fracture water inrush, considering particle loss," *Mine Water and the Environment*, vol. 40, no. 2, pp. 466–478, 2021.

[24] B. H. Yao, L. C. Wang, J. P. Wei, Z. H. Li, and X. J. Liu, "A deformation-seepage-erosion coupling model for water outburst of karst collapse pillar and its application," *Journal of China Coal Society*, vol. 43, no. 7, pp. 2007–2013, 2018.

[25] L. P. Li, S. C. Li, S. S. Shi, and Z. H. Xu, "Water inrush mechanism study of fault activation induced by coupling effect of stress-seepage-damage," *Chinese Journal of Rock Mechanics and Engineering*, vol. 30, pp. 3295–3304, 2011.

[26] A. W. Skempton and J. M. Brogan, "Experiments on piping in sandy gravels," *Geotechnique*, vol. 44, no. 3, pp. 449–460, 1994.

[27] B. Y. Su, M. L. Zhan, and Z. T. Zhang, "Experimental research of seepage characteristic for filled fracture," *Rock and Soil Mechanics*, vol. 15, no. 4, pp. 46–52, 1994.

[28] S. S. Tomlinson and Y. P. Vaid, "Seepage forces and confining pressure effects on piping erosion," *Canadian Geotechnical Journal*, vol. 37, no. 1, pp. 1–13, 2000.

[29] R. J. Fannin and R. Moffat, "Observations on internal stability of cohesionless soils," *Geotechnique*, vol. 56, no. 7, pp. 497–500, 2006.

[30] F. Bendahmane, D. Marot, and A. Alexis, "Experimental parametric study of suffusion and backward erosion," *Journal of Geotechnical and Geoenvironmental Engineering*, vol. 134, no. 1, pp. 57–67, 2008.

[31] D. Marot, F. Bendahmane, F. Rosquoet, and A. Alexis, "Internal flow effects on isotropic confined sand-clay mixtures," *Soil & Sediment Contamination*, vol. 18, no. 3, pp. 294–306, 2009.

[32] H. H. Nguyen, D. Marot, and F. Bendahmane, "Erodibility characterisation for suffusion process in cohesive soil by two types of hydraulic loading," *La Houille Blanche*, vol. 98, no. 6, pp. 54–60, 2012.

[33] J. W. Liang and Y. G. Fan, "Experimental study of seepage characteristics of tiny-particle clay," *Chinese Journal of Rock Mechanics and Engineering*, vol. 29, no. 6, pp. 1222–1230, 2010.

[34] K. S. Richards and K. R. Reddy, "Experimental investigation of initiation of backward erosion piping in soils," *Geotechnique*, vol. 62, no. 10, pp. 933–942, 2012.

[35] O. Y. Mao and T. Akihiro, "Influence of initial fines content on fabric of soils subjected to internal erosion," *Canadian Geotechnical Journal*, vol. 53, no. 2, pp. 299–313, 2016.

[36] Y. Meng, H. Jing, Q. Yin, and X. Wu, "Experimental study on seepage characteristics and water inrush of filled karst structure in tunnel," *Arabian Journal of Geosciences*, vol. 13, no. 12, 2020.

[37] M. X. Wang, W. M. Yang, Z. Q. Zhou et al., "Experimental research on the effect of particle migration of a filling medium in a fault during water and mud inrush," *Arabian Journal of Geosciences*, vol. 14, no. 21, 2021.